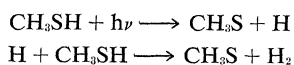


diation. The ultraviolet (280 to 290  $m\mu$ ) and visible bands grow parallelly, suggesting that the two bands arise from the same species. The color is stable for at least 3 to 5 hours at  $-80^\circ\text{C}$ . Though fading is apparent at higher temperatures, color is still detectable after 45 minutes at  $-20^\circ\text{C}$ . In experiments with the water clathrate of  $(\text{CCl}_4, \text{H}_2\text{S})$  color develops with the sample held between  $-10^\circ$  and  $-2^\circ\text{C}$  during irradiation. Color stability here is the order of 1 or 2 minutes.

These observations can be interpreted in terms of reactive species located in cavities of the water clathrate. In the  $\text{CH}_3\text{SH}$  clathrate  $\text{CH}_3\text{S}$  is assumed to be stabilized. This is produced by the following reactions (6):

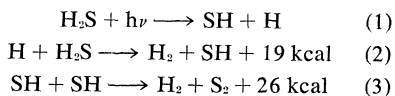


Similarly,  $\text{C}_2\text{H}_5\text{S}$  resides in the cavities of its parent clathrate. Evidence in support of these assignments comes from the work of Rosengren, who shows that photolysis of mercaptans in hydrocarbon glasses at  $77^\circ\text{K}$  produces absorptions with  $\lambda_{\text{max}}$  at 400  $m\mu$  which are assigned to  $\text{RS}$  radicals (7). My experiments in polar glass with  $\text{CH}_3\text{SH}$  provide independent confirmation of Rosengren's results.

The observed temperature stability of the absorption bands reinforces the hypothesis that the radicals occupy clathrate cavities. Though diminished in intensity, the 310- and 370- $m\mu$  bands survive annealing at  $-20^\circ\text{C}$  for 40 minutes.

It is not likely that  $\text{CH}_3\text{S}$  and  $\text{C}_2\text{H}_5\text{S}$  will disproportionate in their cavities. The absorptions assigned here to these radicals are unlike those reported for products of thyl radical disproportionation (8).

In the  $\text{H}_2\text{S}$  clathrates the stabilized species is assumed to be  $\text{S}_2$ . This is produced by the following reactions (9):



The radius of escape from the cavities varies from 1.0 to 1.5  $\text{\AA}$ , depending on cavity size (10).  $\text{SH}$  is too large (radius = 1.7  $\text{\AA}$ ) to diffuse interstitially. After dissociation, however, the products possess sufficient kinetic energy to distort the hydrogen bonded lattice, permitting  $\text{SH}$  to pass from the parent cage into a neighboring one and to react according to reaction 3 (11). Evidence in support of  $\text{S}_2$ , one of the

known products of photolyzed  $\text{H}_2\text{S}$ , as the absorbing species in Fig. 1 is drawn from (i) the maximum in the ultraviolet absorption of Fig. 1 at 280 to 290  $m\mu$  which falls near the position of the strongest absorption bands of the  $\nu', o$  progression of  $\text{S}_2$  (12) and (ii) the absorption band with  $\lambda_{\text{max}} = 507 m\mu$  reported in low temperature deposits of  $\text{S}_2$  (13). This band falls reasonably close to the 520 and 560  $m\mu$  bands of the water clathrates of  $\text{H}_2\text{S}$ . Higher polymers of sulfur (for example,  $\text{S}_6$  and  $\text{S}_8$ ) can probably be ruled out of consideration because their absorption characteristics (14) do not fully satisfy both i and ii.

The stability of color at relatively high temperatures also supports the view that the active species is stabilized in the cavities.

The spectral differences between the single and double water clathrates of  $\text{H}_2\text{S}$  may originate in structural differences between the hydrate types. Single hydrates all form in a cubic lattice of 12  $\text{\AA}$  unit cell edge with two sizes of cavity: 5.2  $\text{\AA}$  and 5.9  $\text{\AA}$  free diameters. The double hydrates form also in a cubic symmetry, of unit cell edge 17.3  $\text{\AA}$ , again with two sizes of cavity: 4.8  $\text{\AA}$  and 6.9  $\text{\AA}$  (15). Thus  $\text{S}_2$  resides in a cavity of different size according to the structure of the water clathrate from which it was formed. Consequently the  $\text{S}_2$  energy levels experience a matrix shift relative to the gas phase spectrum, the magnitude of shift depending on cavity size. Concentrations of stabilized species cannot be given at the present time (16).

PAUL GOLDBERG\*

Department of Physical Chemistry,  
Hebrew University, Jerusalem, Israel

#### References and Notes

- G. C. Pimentel, in *Formation and Trapping of Free Radicals*, A. M. Bass and H. P. Broida, Eds. (Academic Press, New York, 1960), p. 69.
- L. Mandelcorn, *Chem. Revs.* **59**, 827 (1959).
- H. S. Peiser, in *Formation and Trapping of Free Radicals*, A. M. Bass and H. P. Broida, Eds. (Academic Press, New York, 1960), p. 301.
- F. O. Rice, in *Free Radicals in Inorganic Chemistry*, Advances in Chemistry Series 36, (American Chemical Society, Washington, D.C., 1962), p. 3.
- O. H. Griffith and H. M. McConnell, *Proc. Natl. Acad. Sci. U.S.* **48**, 1877 (1962).
- E. W. R. Steacie, *Atomic and Free Radical Reactions* (Reinhold, New York, ed. 2, 1954).
- Kj. Rosengren, *Acta Chem. Scand.* **16**, 1418 (1962).
- , *ibid.*, pp. 1401, 2284.
- R. G. W. Norrish and A. P. Zeelenberg, *Proc. Roy. Soc. London* **A240**, 293 (1957).
- Computed from the crystallographic data of L. Pauling and R. E. Marsh [*Proc. Natl. Acad. Sci. U.S.* **38**, 112 (1952)] and the value of 1.40  $\text{\AA}$  as the Van der Waals radius of oxygen.
- The radii of  $\text{CH}_3\text{S}$  and  $\text{C}_2\text{H}_5\text{S}$  are estimated to be 2.4 and 3.1  $\text{\AA}$ , respectively. These radicals are probably too large to move from

their parent cages by the mechanism proposed for  $\text{SH}$ .

- G. Herzberg and L. G. Mundie, *J. Chem. Phys.* **8**, 263 (1940).
- B. Meyer and E. Schumacher, *Helv. Chim. Acta* **43**, 1333 (1960); *Nature* **186**, 801 (1960).
- P. D. Bartlett, G. Lohaus, C. D. Weis, *J. Am. Chem. Soc.* **80**, 5064 (1958).
- M. von Stackelberg, *Rec. Trav. Chim. Pays-Bas* **75**, 902 (1956); H. R. Muller and M. von Stackelberg, *Naturwissenschaften* **39**, 20 (1952).
- I express gratitude and thanks to Prof. G. Stein of the Hebrew University, Jerusalem, Israel, not only for many helpful discussions and valuable suggestions but also for providing the stimulating academic environment in which this work was done. Dr. A. Treinin, Dr. M. Ottolenghi, and Prof. O. Schnepp provided valuable advice. Research supported by fellowship CSP-15,658 from the National Cancer Institute.
- \* Present address: General Telephone and Electronics Laboratories, Bayside 60, N.Y.

9 August 1963

## Coesite and Shocked Quartz from Holleford Crater, Ontario, Canada

Abstract. *The Holleford Crater, a circular depression in southern Ontario, is filled with Paleozoic sediments and underlain by brecciated Precambrian igneous and metamorphic rocks. The presence of coesite in two core samples of this breccia has been established by petrographic and x-ray diffraction methods. Shattered quartz in the coesite-bearing samples exhibits planar fractures. The shocked quartz is the result of great shock pressures and the association of coesite with the shocked quartz strongly suggests that Holleford Crater originated from a hypervelocity impact.*

Holleford Crater is located approximately 25.7 km. (16 mi) north of Kingston, and 132 km (82 mi) southwest of Ottawa, Ontario, Canada (1). This circular depression was first recognized by Beals, Ferguson, and Landau in a systematic search of aerial photographs of various regions in Canada (2). In 1956–57, Beals directed a comprehensive study of the crater by geological and geophysical methods. This study included drilling three diamond drill holes that successively penetrated Paleozoic limestone, consolidated breccia, and Precambrian plutonic rocks, as described by Beals (2) who made available the core samples used in this investigation. The crater, 2.35 km (1.46 mi) in diameter and 30.5 m (100 ft) deep, is in Precambrian rock. Several hundred feet of breccia lies in a bowl-shaped depression in the Precambrian rock surface and is overlain by Paleozoic sediments. Beals estimates the age of the crater

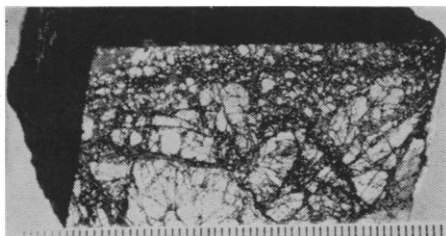


Fig. 1. Polished surface of shattered, coesite-bearing quartz (sample 737). Scale in millimeters.

as between 5 and 6 hundred million years. The crater features are obscured by erosion and post-impact deposition.

Portions of selected core specimens were crushed and examined optically, by oil immersion methods. Traces of coesite were recognized in core samples from hole 2 at depths of 214.6 and 224.6 m (704 and 737 ft). For convenience of reference, these samples are designated 704 and 737. These two samples were further disaggregated and sieved into various grain-size fractions. The fine fraction (-325 mesh) was treated in an acid solution (5 percent HF, 5 percent HNO<sub>3</sub>, 1:1 HCl) at 25°C for 86 hours. The residue, after this treatment, consisted of quartz rutile, and coesite. The presence of coesite from samples 704 and 737 was confirmed by x-ray powder diffraction. From the powder pattern, there are eight coesite lines, including the three most intense, that are not coincident with lines produced by other material in the residue (see Table 1).

The Holleford coesite has a mean refractive index of 1.593, very low birefringence, and strain characteristic of impact-produced coesite. Because of the limited occurrence of coesite in the samples analyzed and its fine grain size, coesite from Holleford has not been identified in thin-section study.

The establishment of the presence of coesite in Holleford Crater is significant for three reasons: it strengthens earlier suggestions that the Holleford

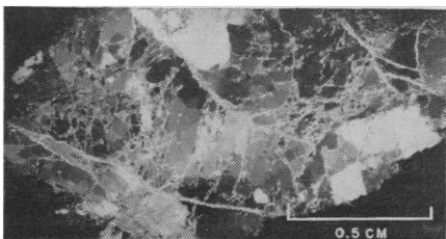


Fig. 2. Photomicrograph of a thin section of quartz (sample 737) illustrating plastic deformation and fracturing along two major fault planes. Crossed nicols.

structure is a meteorite impact crater, it is the oldest occurrence of coesite known at this time, and it establishes the fact that coesite may persist, at least in part, in a moderate temperature-pressure environment throughout geologic time. Dachille and Roy (3), in an experiment devised to determine the metastable persistence of coesite and stishovite, found that coesite will persist at a temperature of 1100°C at least for weeks and is much less likely to revert to other forms of SiO<sub>2</sub> than is stishovite, dependent upon other factors such as grain size, pressure and environmental history.

The polymict breccia of sample 704 represents angular rock fragments of lime-silicate rocks, amphibolite, gneiss, and quartz. The matrix, light green in color, is medium to fine grained and contains quartz, calcite, pyrite, amphibole, chlorite, and clay minerals.

Sample 737 is essentially smoky quartz that has been intensely shattered (Fig. 1) and contains minor amounts of chlorite, muscovite, clay minerals, and a trace of apatite. Chlorite and muscovite occur as fracture fillings. Pale, apple green lime-silicate rock borders the smoky quartz on both sides in the core section. The mineral composition of the lime-silicate material is predominantly quartz and diopside with minor amounts of calcite, mica, and pyrite. There are several shear zones occupied by granulated quartz, diopside, and calcite.

A petrographic study of the shattered coesite-bearing quartz, sample 737, revealed that the quartz was deformed by fracturing, predominantly along rational crystallographic planes. These cleavage fractures in order of decreasing abundance are commonly parallel to the unit rhombohedron *r*, the prism *m*, and the basal plane *c*. This is in close agreement with data (4) for observations of natural cleavage in quartz. Christie, Heard, and La Mori (5) report that the development of cleavage fracture in quartz as a result of quartz deformation in a piston and cylinder device at 27 to 30 kilobars confining pressure took place with greater facility on *c*, *r*, *z* and rarely on *m* and *a*. Their quartz samples failed by rupture along "faults" in planes of high-shear stress and they suggest that the faulting is a fracture phenomenon that developed from small amounts of slip on crystallographic planes; this initiated submicroscopic cracks which grew large enough to propagate as brittle fractures.

Table 1. Comparison of x-ray diffraction powder data (d spacing and intensity) between Holleford coesite (as found in this study) and synthetic coesite as found by Boyd and England (7).

Synthetic coesite		Holleford coesite	
d(Å)	Intensity	d(Å)	Intensity*
6.19	3	6.19	VVW
4.37	2		
3.436	52	3.43	M
3.099	100	3.10	S
2.765	8	2.76	W
2.698	11	2.69	W
2.337	3		
2.295	6		
2.186	4		
2.033	6		
1.849	5	1.85	VW
1.839	3		
1.794	4		
1.787	4		
1.715	9		
1.698	10	1.70	W
1.655	6		
1.584	5		
1.409	2		
1.345	6	1.35	VW

\* Intensity: VVW, very very weak; M, moderate; S, strong; W, weak; VW, very weak.

There are many fractures that are not parallel to the more common crystallographic planes; these are commonly inclined at low angles to {0001}. Many of these fractures have developed along Böhm lamellae and terminate rather abruptly.

In addition to the planar structures that have been described, several shear faults occur in single crystals within the shattered specimen. The areas bordering the fault planes show evidence of plastic deformation and fracturing in response to drag movement along the fault plane (Fig. 2). The shear faults closely parallel crystallographic planes in quartz but the precise relationship of the fault planes with crystallographic planes is difficult to determine because of varying degrees of rotation and fracturing of the crystal along the fault plane.

The mutual association of the high-pressure SiO<sub>2</sub> polymorph coesite, and the strongly deformed quartz suggests that the cleavage fractures are the result of great shock pressure and are similar to experimentally deformed quartz in mode of development. The term shocked quartz is presented here to describe highly deformed quartz that has ruptured in response to high pressure developed by meteorite impact, or possibly by other shock mechanisms.

T. E. BUNCH

Mellon Institute, Pittsburgh

ALVIN J. COHEN

Department of Earth and Planetary Sciences, University of Pittsburgh, Pittsburgh, Pennsylvania

## References and Notes

1. This paper was presented in part at the First Western National Meeting of the American Geophysical Union, Los Angeles, 27-29 December 1961, Abstr. *J. Geophys. Res.* **67**, 1630a (1962).
2. C. S. Beals, *Publ. Dominion Obs.* Ottawa, **24**, No. 6 (1960).
3. F. Dacheille and R. Roy, *Geol. Soc. Am. Annual Meeting, Abstr.* (1962), p. 34A.
4. H. W. Fairbairn, *Am. Mineralogist* **24**, 365 (1939).
5. J. M. Christie, H. C. Heard, P. N. La Mori, *Am. J. Sci.*, in press.
6. We thank Dr. C. S. Beals of the Dominion Observatories, Ottawa, Canada, for making available the core samples used in this investigation. This work was supported by grant NsG-57-60, supplement 1-62, from the National Aeronautics and Space Administration.
7. F. R. Boyd and J. L. England, *J. Geophys. Res.* **65**, 749 (1960).

24 June 1963

## Radar Observations of Mercury

Subsequent to the radar observations of Venus (1) and Mars (2), similar observations have now been made of Mercury during its recent conjunction in May. This latter series of measurements was made at the Jet Propulsion Laboratory's Goldstone tracking station, located in the Mojave desert of California. Mercury was illuminated with 100 kw of power at a wave length of 12.5 cm. An 85-ft parabolic antenna was used alternately for both transmission and reception.

The same techniques were used for the three different types of signal processing as were used for the data obtained for Venus (1), so that the two sets of data may be compared directly. In the simplest type of processing, the receiver was used in the configuration of a Dicke radiometer (except that the transmitter was keyed instead of the receiver), and the total power of the echo was measured. Typically, signals obtained over 4 hours were integrated. The measured value of the signal power

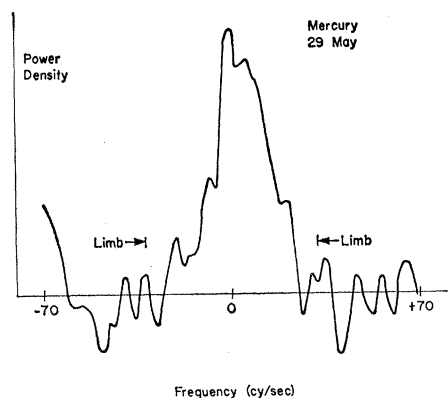


Fig. 1. A spectrogram showing data obtained for Mercury during 2 hours of signal integration.

18 OCTOBER 1963

was eleven times the root mean square of the fluctuations, which are caused by noise. This high-confidence measurement was made upon a signal of only  $5 \times 10^{-22}$  watt. The radar cross section of Mercury was measured as 5 percent of its geometric cross section. This compares with 10 percent for Venus and 3 percent for Mars.

In the second type of data processing, the power of the echo was analyzed into its frequency components by means of the autocorrelation function approach. A wave of high spectral purity was transmitted to Mercury, but the echo was both shifted and broadened in frequency by the Doppler effect. The shift was caused by the relative orbital velocity between Mercury and the radar station; the broadening was caused by the apparent rotation, which imparts differing velocities along the lines of sight to different parts of the surface.

In Fig. 1, the lines marked above the abscissa show the calculated position of echoes reflected from the limbs of Mercury; echoes are detected almost to the limbs. This corroborates our conclusions that Venus undergoes a slow retrograde rotation, for such a conclusion requires that Venus echoes (which are much stronger) be detectable near the limbs.

The width of the spectrograms, in relation to the size and rotation of Mercury, gives a measure of the roughness of its surface. In this sense Mercury is much rougher than Mars and perhaps twice as rough as Venus. The Doppler shift of the signal was removed by an ephemeris-tuned receiver, hence the frequency of the central part of the spectrograms gives directly the velocity errors of the ephemeris. Table 1 shows a list of these residuals.

In the third type of data processing a spectrometer was used to analyze the signal selected by a range-gate. The transmitter was modulated with a wide-band waveform. The range-gate was set to accept echoes from a specified 178-km zone of Mercury, and to reject all others (Fig. 2). The selected signal was then analyzed for its frequency content.

Since these echoes originate from known areas on Mercury, its speed of rotation may be inferred. Of course, it has long been known that the period of Mercury's rotation is 88 days; but the measurement, which was in excellent agreement, serves as an effective check on one of the techniques we used to measure the rotation of Venus.

Table 1. Residuals calculated for Mercury.

Date	Velocity (cm/sec)	Range (meters)
5/15/63	-28	
5/16/63	-20	
5/21/63	-49	
5/23/63	-44	
5/24/63		+1.1 $10^5$
5/25/63	-38	
5/26/63	-25	
5/28/63	-22	+1.7 $10^5$
5/29/63	-22	

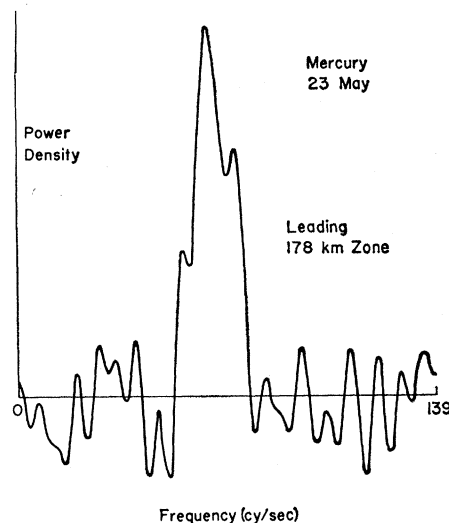


Fig. 2. A spectrogram showing data obtained for Mercury by means of a spectrometer in which the range was restricted with a range-gate set to accept echoes only from a specified 178-km zone.

From spectrograms of this type we also measured the time taken by a radar signal to get to Mercury and back, and hence the distance. The internal consistency of this method was good to within 15 km. Since the orbital velocity of Mercury carries it through one range zone in only a dozen seconds, it is necessary to control the range-gate with an ephemeris also. Thus the range-gated spectrograms give the range error of the ephemeris. These residuals are also presented in Table 1.

The trends seen in these data are essentially eliminated by adjusting the argument of the ephemeris by only 6 seconds, and the astronomical unit by only  $10^5$  meters. These data provide a striking confirmation of the astronomical unit reported by Muhleman (3) of this laboratory, which was based on radar observations of Venus during the conjunctions of 1961 and 1962.

ROLAND L. CARPENTER  
RICHARD M. GOLDSTEIN

*Jet Propulsion Laboratory, California Institute of Technology, Pasadena*